Letters

Transient Synchronization Stability Improvement Control Strategy for Grid-Connected VSC Under Symmetrical Grid Fault

Sen Huang, Jun Yao, *Member, IEEE*, Jinxin Pei, Shiyue Chen, Yi Luo, and Zhaoyang Chen

***Abstract*—Under grid fault, the grid-connected voltage source converters (VSCs) have the risk of transient synchronization instability during low voltage ride through. Based on the equivalent rotor swing equation of VSC, this letter proposes an improved transient synchronization stability control strategy, which improves the existence of equilibrium points and transient synchronization behaviors of the VSC system. Thus, the transient synchronization stability of grid-connected VSC can be significantly enhanced. The simulation and experimental results demonstrate the validity of the proposed strategy.**

***Index Terms*— Grid fault, improvement control strategy, transient synchronization stability.**

NOMENCLATURE

$\boldsymbol{U}_{\mathbf{g}}$, $\boldsymbol{U}_{\mathbf{t}}$, $\boldsymbol{I}$	Vectors of grid voltage, terminal voltage, and output current of VSC, respectively.
R_{g}, L_{g}, $\boldsymbol{Z}_{\mathrm{g}}$	Resistance, inductance, and impedance of the transmission line, respectively.
ω_{g}, ω_{PLL}, ω_{b}	Grid voltage vector's angular frequency, PLL's output angular frequency, and angular frequency base value, respectively.
δ	Phase angle difference between PLL's *d*-axis reference frame and grid voltage vector $\boldsymbol{U}_{\mathbf{g}}$.
U_{dc}	DC-link voltage.
k_{p}, k_{i}	PI coefficients of the PLL, respectively.
k_{pf}, k_{if}	PI coefficients of the AVR, respectively.
J_{v}, D_{v}	Virtual inertia and virtual damping, respectively.
T_{v}^{*}, T_{v}	Virtual prime mover torque and virtual output torque, respectively.
J_{va}, D_{va}, T_{va}	Additional virtual inertia coefficient, virtual damping coefficient, and virtual output torque generated by AVR, respectively.
C_{f}, L_{f}	Filter capacitor and filter inductance, respectively.

Manuscript received September 22, 2021; revised October 28, 2021; accepted November 25, 2021. Date of publication November 30, 2021; date of current version January 19, 2022. This work was supported in part by the National Natural Science Foundation of China under Grant 51977019, in part by Joint Research Fund in Smart Grid under Grant U1966208 under Cooperative Agreement between the National Natural Science Foundation of China and State Grid Corporation of China, and in part by the 111 Project of China under Grant B18062. *(Corresponding author: Jun Yao.)*

Sen Huang, Jun Yao, Shiyue Chen, Yi Luo, and Zhaoyang Chen are with the State Key Laboratory of Power Transmission Equipment and System Security and New Technology, School of Electrical Engineering, Chongqing University, Chongqing 400044, China (e-mail: huangsenwarm@163.com; topyj@163.com; csy_chenshiyue@163.com; 835889603@qq.com; yyy371424@qq.com).

Jinxin Pei is with Chongqing Jialing Huaguang Photoelectric Technology Co., Ltd., Chongqing 400700, China (e-mail: peijinxindoc@163.com).

Color versions of one or more figures in this article are available at https://doi.org/10.1109/TPEL.2021.3131361.

Digital Object Identifier 10.1109/TPEL.2021.3131361

I. INTRODUCTION

In recent years, to cope with the energy crisis and environmental pollution, renewable energy generation technology with grid-connected voltage source converters (VSCs) as the interface for wind turbine and photovoltaic has been rapidly developed. To improve the secure and stable operation of the power system, the grid codes have been issued to require VSC to maintain a connection with the grid and inject reactive current to support grid voltage under symmetrical grid faults [1]. However, it is not easy for VSC to synchronize with the grid under such circumstances. Therefore, the transient synchronization stability issue of VSC has attracted great attention. The existing studies [2]–[4], respectively, applied the voltage-vector-triangle graphic method, phase portraits, and quasi-static model to analyze the transient synchronization characteristics of VSC during low voltage ride through (LVRT) and pointed out that the lack of equilibrium point would cause VSC to lose synchronization with the grid. In addition, by studying the VSC's transient synchronization process, He *et al.* [5] and Liu *et al.* [6] indicated that even if the equilibrium point exists, poor transient synchronization behaviors would still lead to the loss of synchronism (LOS). To quantitatively analyze the transient synchronization issue of VSC, the existence of equilibrium point criterion and equivalent equal area criterion (EAC) was proposed in [7], respectively, which can quantitatively calculate the transient stability margin of the system.

In addition to the analytical methods, some control strategies are also presented to enhance the VSC's transient synchronization stability. Göksu *et al.* [2] and He *et al.* [5] proposed to introduce the angular frequency deviation of phase-locked loop (PLL) into the active current or power instruction to adaptively adjust the stability, but they are highly susceptible to the converter capacity restriction. A PLL enhanced control strategy based on additional damping is adopted in [6], which can improve the transient synchronization process, but it only works when equilibrium point exists. In [8], an optimal current proportional control scheme based on line resistance–inductance ratio is proposed, which can ensure that the system has the maximum stability margin, but how to accurately obtain line impedance information in a short time is not easy.

To overcome the limitations of the above approaches, this letter presents a novel automatic voltage regulation (AVR) control strategy. By adding an additional *q*-axis component of the terminal voltage, the AVR can automatically adjust the PLL's input variable and improve the synchronization operating status of the VSC system during grid fault, which can effectively enhance its transient synchronization stability.

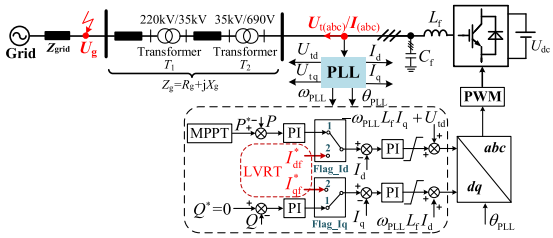

Fig. 1. Diagram of grid-connected VSC.

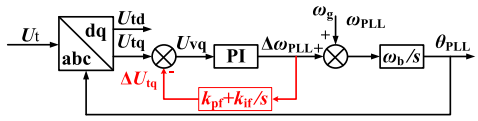

Fig. 2. Diagram of AVR.

II. Proposed Transient Synchronization Stability Control Strategy

A. Equivalent Rotor Swing Equation

A typical grid-connected VSC system is given in Fig. 1. Rotor swing equation is a classic mathematical model for synchronous stability analysis of synchronous generator (SG), which can provide a reference for the study of PLL-based VSC's transient synchronization stability. According to the article presented in [7], the equivalent rotor swing equation of the PLL-based VSC system during LVRT can be expressed as

$$\begin{cases} \frac{J_{\rm v}d\omega_{\rm PLL}}{dt}=T_{\rm v}^*-T_{\rm v}-D_{\rm v}(\omega_{\rm PLL}-\omega_{\rm g}) \\ T_{\rm v}^*=0,\quad T_{\rm v}=U_{\rm g}\sin\delta-\omega_{\rm g}L_{\rm g}I_{\rm df}^*-R_{\rm g}I_{\rm qf}^* \\ J_{\rm v}=\frac{1-k_{\rm p}L_{\rm g}I_{\rm df}^*}{k_{\rm i}},\quad D_{\rm v}=\frac{k_{\rm p}U_{\rm g}\omega_{\rm b}}{k_{\rm i}}\cos\delta-L_{\rm g}I_{\rm df}^*. \end{cases} \tag{1}$$

Equation (1) depicts that the VSC's equivalent rotor swing equation has the same form as that of SG. There is a similarity between VSC and SG in the mathematical model when describing synchronization characteristics. The SG's synchronization stability is affected by the unbalanced torque term. Similarly, the torque deviation ($T_{\rm v}^*-T_{\rm v}$) also has an impact on VSC's synchronization stability. As for $J_{\rm v}$ and $D_{\rm v}$, which represent the anti-disturbance ability. In addition, $J_{\rm v}$ can be approximately regarded as a constant, while $D_{\rm v}$ can be considered as a function of equivalent power angle (EPA) δ during LVRT [7]. Especially, only if $D_{\rm v}>0$, the negative feedback regulation of $\omega_{\rm PLL}$ can be realized.

B. Proposed Control Strategy

For grid-following VSC, PLL is the key to realize grid-connected synchronization. By controlling the input variable $U_{\rm tq}$ to zero, PLL can accurately track grid voltage $\boldsymbol{U_{\rm g}}$, and then the VSC can realize subsequent control. However, if $|R_{\rm g}I_{\rm qf}^*+\omega_{\rm g}L_{\rm g}I_{\rm df}^*|$ is greater than $|\boldsymbol{U_{\rm g}}|$ due to inappropriate current instruction, $U_{\rm tq}$ cannot be controlled to zero (i.e., $T_{\rm v}^*\neq T_{\rm v}$), which would lead to non-equilibrium instability of the system. In addition, even if the system has equilibrium point, it is not easy to maintain $U_{\rm tq}$ equal to zero owing to poor transient behaviors, and the system would still be unstable.

In short, controlling the input variable of PLL to zero stably determines the transient synchronization stability of the VSC. Therefore, in order to realize this control objective, an improved PLL control strategy based on AVR is proposed in this letter. As shown in Fig. 2, the AVR generates an additional q-axis component of the terminal voltage $\Delta U_{\rm tq}$ through the frequency deviation $\Delta\omega_{\rm PLL}$, which can automatically adjust the input variable $U_{\rm vq}$ of the PLL, thereby improving the transient control performance of the VSC system.

With AVR, the input variable of the PLL during LVRT can be expressed as

$$\begin{cases} U_{\rm vq}=-U_{\rm g}\sin\delta+R_{\rm g}I_{\rm qf}^*+\omega_{\rm PLL}L_{\rm g}I_{\rm df}^*-\Delta U_{\rm tq} \\ \Delta U_{\rm tq}=k_{\rm pf}\Delta\omega_{\rm PLL}+k_{\rm if}\int\Delta\omega_{\rm PLL}dt. \end{cases} \tag{2}$$

Equation (2) shows that if $\omega_{\rm PLL}$ deviates from $\omega_{\rm g}$, the AVR would automatically generate $\Delta U_{\rm tq}$ to adjust the input variable $U_{\rm vq}$ of the PLL. Hence, after AVR is adopted, the equivalent rotor swing equation of VSC during LVRT becomes

$$\begin{cases} (J_{\rm v}+J_{\rm va})\frac{d\omega_{\rm PLL}}{dt}=T_{\rm v}^*-(T_{\rm v}+T_{\rm va})-(D_{\rm v}+D_{\rm va})(\omega_{\rm PLL}-\omega_{\rm g}) \\ T_{\rm v}^*=0, T_{\rm v}=U_{\rm g}\sin\delta-\omega_{\rm g}L_{\rm g}I_{\rm df}^*-R_{\rm g}I_{\rm qf}^*, T_{\rm va}=k_{\rm if}\int\Delta\omega_{\rm PLL}dt \\ J_{\rm v}=\frac{1-k_{\rm p}L_{\rm g}I_{\rm df}^*}{k_{\rm i}}, J_{\rm va}=\frac{k_{\rm p}k_{\rm pf}}{k_{\rm i}} \\ D_{\rm v}=\frac{k_{\rm p}U_{\rm g}\omega_{\rm b}\cos\delta}{k_{\rm i}}-L_{\rm g}I_{\rm df}^*, D_{\rm va}=k_{\rm pf}+\frac{k_{\rm p}k_{\rm if}}{k_{\rm i}}. \end{cases} \tag{3}$$

Under the action of AVR, it can be seen from (3) that the virtual inertia and damping coefficient of the VSC have been significantly increased with stronger anti-disturbance ability. More importantly, the additional virtual output torque term $T_{\rm va}$ can autonomously adjust the virtual output torque value according to the frequency deviation. As a result, the system can automatically find the equilibrium point after large disturbances and has the ability to adaptively balance the $T_{\rm v}$ and the $T_{\rm v}^*$, which means the VSC's transient synchronization stability can be significantly improved. The detailed analysis considering the impact of AVR on the VSC's equilibrium point and transient synchronization behaviors is given in Sections II-D and II-E.

C. Design of the AVR's Parameters

Selecting $\Delta\delta$ and $\Delta\omega_{\rm PLL}$ as state variables, and linearizing (3) at the equilibrium point $\delta_{\rm k}$, the small-signal state-space equation of VSC with AVR can be deduced as

$$\begin{bmatrix} \Delta\dot{\delta} \\ \Delta\dot{\omega}_{\rm PLL} \end{bmatrix}=\begin{bmatrix} 0 & \omega_{\rm b} \\ -\frac{S_{\rm Eqa}|_{\delta_{\rm k}}}{J_{\rm v}+J_{\rm va}} & -\frac{(D_{\rm v}+D_{\rm va})|_{\delta_{\rm k}}}{J_{\rm v}+J_{\rm va}} \end{bmatrix}$$
$$\begin{bmatrix} \Delta\delta \\ \Delta\omega_{\rm PLL} \end{bmatrix}=\boldsymbol{A}_{\rm a}\begin{bmatrix} \Delta\delta \\ \Delta\omega_{\rm PLL} \end{bmatrix} \tag{4}$$

where $S_{\rm Eqa}=U_{\rm g}\cos\delta+k_{\rm if}/\omega_{\rm b}$, and $S_{\rm Eqa}$ can be defined as the equivalent synchronization torque coefficient. Then, the characteristic equation and damping ratio ξ of VSC under the action of AVR can be, respectively, expressed as

$$|\lambda\boldsymbol{E}-\boldsymbol{A}_{\rm a}|=\lambda^2+\lambda\frac{D_{\rm v}|_{\delta_{\rm k}}+D_{\rm va}}{J_{\rm v}+J_{\rm va}}+\frac{\omega_{\rm b}}{J_{\rm v}+J_{\rm va}}S_{\rm Eqa}|_{\delta_{\rm k}}=0 \tag{5}$$

$$\xi=\frac{k_{\rm p}U_{\rm g}\omega_{\rm b}\cos\delta_{\rm k}-k_{\rm i}L_{\rm g}I_{\rm df}^*+(k_{\rm i}k_{\rm pf}+k_{\rm p}k_{\rm if})}{2\sqrt{(1-k_{\rm p}L_{\rm g}I_{\rm df}^*+k_{\rm pf}k_{\rm p})k_{\rm i}(U_{\rm g}\omega_{\rm b}\cos\delta_{\rm k}+k_{\rm if})}}. \tag{6}$$

According to the control theory, when the damping ratio is 0.707, the stability and dynamic response rate of the system reach the comprehensive optimum. Therefore, the optimum damping ratio $\xi_{\rm op}$ ($\xi=0.707$) can be used as the design principle of the AVR controller parameters. However, it is worth mentioning that in the actual selection of parameters, as long as the damping ratio can be as close to $\xi_{\rm op}$ as

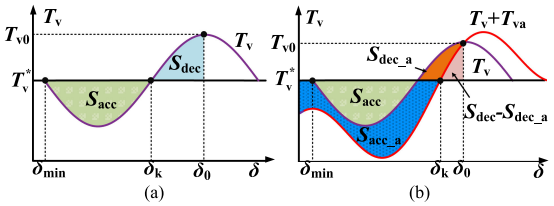

Fig. 3. Transformation relationship of acceleration and deceleration areas when $T_{v0}>T_v^*$. (a) Without AVR. (b) With AVR.

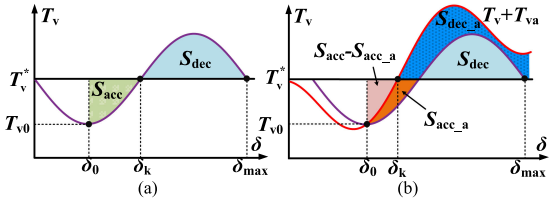

Fig. 4. Transformation relationship of acceleration and deceleration areas when $T_{v0} < T_v^*$. (a) Without AVR. (b) With AVR.

possible, AVR can significantly improve the transient stability of the system. Therefore, AVR has strong adaptability.

D. Impact of AVR on the Equilibrium Point

The existence of equilibrium point is a prerequisite for the VSC system to achieve transient synchronization stability. The impact of AVR on the equilibrium point can be discussed as follows.

1) $T_v^*>T_v$: When the VSC system lacks equilibrium point due to insufficient T_v, the excess T_v^* would drive ω_{PLL} to accelerate, making $\Delta\omega_{PLL}>0$. The T_v can only reduce the unbalanced virtual torque difference by increasing δ [7]. However, according to (3), with AVR, $\Delta\omega_{PLL}>0$ would inevitably cause $k_{if}\int\Delta\omega_{PLL}dt$ to increase, resulting in $T_{va}>0$. T_{va} would be used as an additional torque term to make up for the shortage of T_v and promote the system to find a new equilibrium point.
2) $T_v^* < T_v$: When the VSC system does not exist equilibrium point due to insufficient T_v^*, the excess T_v would force ω_{PLL} to decelerate and make $\Delta\omega_{PLL}<0$. So that T_v needs to reduce δ to balance T_v^*. With AVR, $\Delta\omega_{PLL}<0$ would cause a decrease in T_{va} to counteract the excess T_v and eliminate unbalanced virtual torque difference, thus, significantly improving the existence of equilibrium point.

E. Impact of AVR on the Transient Synchronization Behavior

However, even though the equilibrium point exists, the VSC system may fail to reach the desired equilibrium point due to poor transient synchronization behaviors during LVRT. Therefore, refer to the article presented in [7], using equivalent EAC to analyze the transient synchronization behavior of VSC.

1) $T_{v0}>T_v^*$: As shown in Fig. 3(a), when the initial torque value T_{v0} is greater than T_v^*, the system would experience a process of decelerating first and then accelerating. Under such circumstance, the equivalent EAC during LVRT can be expressed as

$$\begin{cases} S_{dec}=\int_{\delta_k}^{\delta_0}(T_v-T_v^*)d\delta, \quad S_D=\frac{1}{\omega_b}\int_{\delta_{min}}^{\delta_0}D_v d\delta \\ \max\{S_{acc}\}=\int_{\delta_{min}}^{\delta_k}(T_v^*-T_v)d\delta \\ S_{dec}\le\max\{S_{acc}\}+S_D \end{cases} \tag{7}$$

where δ_0 and δ_k are the EPA corresponding to the initial time and the desired equilibrium point. δ_{min} and δ_{max} are the transient synchronization stability boundary. S_{dec}, S_{acc}, and S_D represent the equivalent deceleration area, equivalent acceleration area, and virtual damping energy, respectively. Criterion (7) indicates that only when the sum of the maximum S_{acc} and S_D is greater than S_{dec}, the VSC system can maintain transient energy balance. Otherwise, the VSC would lose synchronization with the grid and the LOS for angular frequency dropping would occur.

When the proposed AVR is adopted, the equivalent rotor swing equation changes from (1) to (3). The equivalent EAC of VSC becomes

$$\begin{cases} S_{dec}-S_{dec\_a}=\int_{\delta_k}^{\delta_0}(T_v-T_v^*)d\delta-\left|\int_{\delta_k}^{\delta_0}T_{va}d\delta\right| \\ S_D+S_{D\_a}=\frac{1}{\omega_b}\int_{\delta_{min}}^{\delta_0}D_v d\delta+\frac{1}{\omega_b}\int_{\delta_{min}}^{\delta_0}D_{va}d\delta \\ \max\{S_{acc}+S_{acc\_a}\}=\int_{\delta_{min}}^{\delta_k}(T_v^*-T_v)d\delta+\left|\int_{\delta_{min}}^{\delta_k}T_{va}d\delta\right| \\ S_{dec\_a}-S_{dec\_a}\le\max\{S_{acc}+S_{acc\_a}\}+S_D+S_{D\_a}. \end{cases} \tag{8}$$

According to Criterion (8) and Fig. 3(b), due to the adaptive adjustment of T_{va}, the equivalent deceleration area of the system is reduced, while the maximum acceleration area is significantly increased, which means that the transient stability margin of the system is increased. In addition, the existence of D_{va} increases the virtual damping coefficient of the system, which can consume more unbalanced energy in the transient process. Therefore, the transient synchronization stability of the VSC system during LVRT can be enhanced.

2) $T_{v0}<T_v^*$: As shown in Fig. 4(a), when T_{v0} is less than T_v^*, the system would experience a process of accelerating first and then decelerating. Therefore, the equivalent EAC during LVRT can be derived as

$$\begin{cases} S_{acc}=\int_{\delta_0}^{\delta_k}(T_v^*-T_v)d\delta, \quad S_D=\frac{1}{\omega_b}\int_{\delta_0}^{\delta_{max}}D_v d\delta \\ \max\{S_{dec}\}=\int_{\delta_k}^{\delta_{max}}(T_v-T_v^*)d\delta \\ S_{acc}\le\max\{S_{dec}\}+S_D. \end{cases} \tag{9}$$

If Criterion (9) is not met, the VSC would lose synchronization with the grid and the LOS for angular frequency rising would occur.

With AVR, the equivalent EAC of VSC becomes

$$\begin{cases} S_{acc}-S_{acc\_a}=\int_{\delta_0}^{\delta_k}(T_v^*-T_v)d\delta-\left|\int_{\delta_k}^{\delta_0}T_{va}d\delta\right| \\ S_D+S_{D\_a}=\frac{1}{\omega_b}\int_{\delta_0}^{\delta_{max}}D_v d\delta+\frac{1}{\omega_b}\int_{\delta_0}^{\delta_{max}}D_{va}d\delta \\ \max\{S_{dec}+S_{dec\_a}\}=\int_{\delta_k}^{\delta_{max}}(T_v-T_v^*)d\delta \\ +\left|\int_{\delta_k}^{\delta_{max}}T_{va}d\delta\right| \\ S_{acc}-S_{acc\_a}\le\max\{S_{dec}+S_{dec\_a}\}+S_D+S_{D\_a}. \end{cases} \tag{10}$$

According to Fig. 4(b) and Criterion (10), due to AVR, not only equivalent acceleration area is reduced but also the maximum equivalent deceleration area and virtual damping energy are significantly increased. Hence, the transient stability of the system is also improved under this circumstance.

It should be noted that under normal grid condition, small disturbances would also cause the existing proportional–integral (PI) controller output angular frequency deviation $\Delta\omega_{PLL}$, which would make AVR output ΔU_{tq}, thereby affecting the input of the existing PI controller. This would vary the virtual output torque characteristics of the VSC and affect its status, which may make it difficult to operate in unit power factor mode. Therefore, the AVR strategy is only enabled under grid fault.

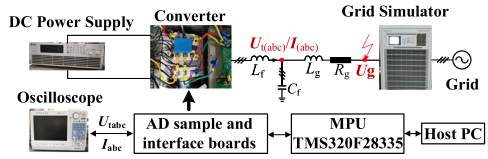

Fig. 5. Configuration of the grid-connected VSC system.

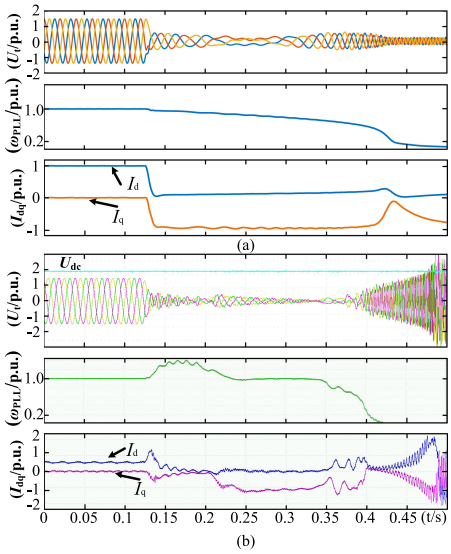

Fig. 6. Simulation and experimental results of Case 1. (a) Simulation verification. (b) Experimental verification.

III. Simulation and Experimental Validation

To verify the effectiveness of the proposed AVR strategy, the simulation and experimental verification are carried out in this section. The simulated system and experimental set-up are configured as Figs. 1 and 5, respectively, and their main parameters are given in Tables I and II of the Appendix.

Case 1: When the grid voltage symmetrically drops to 0.05 p.u., I_{df}^{*} and I_{qf}^{*} are set to 0 p.u. and -1.0 p.u., respectively. According to (1), $T_{\mathrm{v}}^{*}<T_{\mathrm{v}}$, so there is no equilibrium point existing in the VSC system. As illustrated in Fig. 6, the unbalanced torque causes the ω_{PLL} to decrease quickly from 1.0 to 0 p.u. Therefore, the LOS phenomenon for angular frequency dropping occurs due to the lack of equilibrium point.

Case 2: To address the LOS issue of Case 1, the proposed AVR is adopted. As shown in Fig. 7, the VSC system avoids the LOS phenomenon. AVR enables the VSC system to transition to a new stable equilibrium point, making the ω_{PLL} quickly restore to 1.0 p.u. after a rapid transient adjustment.

Case 3: When the grid voltage drops to 0.1 p.u., I_{df}^{*} and I_{qf}^{*} are set to 0 and -0.9 p.u., respectively. Based on (1), there are equilibrium points for the VSC system. However, according to Criterion (7) proposed in [7], the transient energy of the VSC system is unbalanced under such condition, which means that the instability incident cannot be avoided. As shown in Fig. 8, the insufficient acceleration area results in the ω_{PLL} decreasing gradually. Thus, the LOS phenomenon for angular frequency dropping occurs again due to poor transient synchronization behavior.

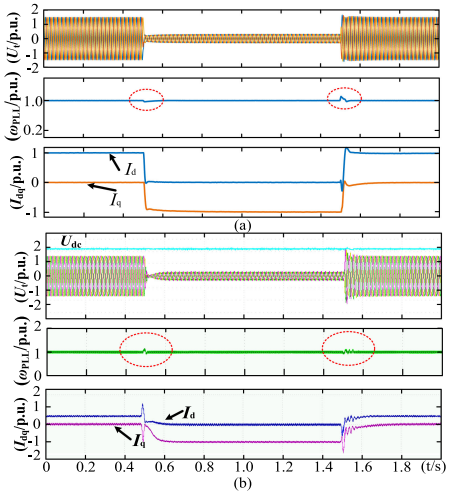

Fig. 7. Simulation and experimental results of Case 2. (a) Simulation verification. (b) Experimental verification.

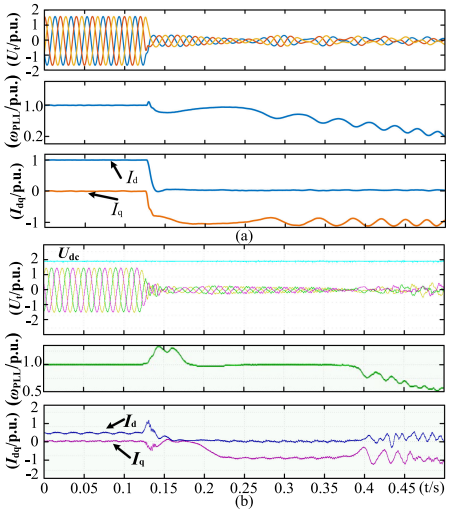

Fig. 8. Simulation and experimental results of Case 3. (a) Simulation verification. (b) Experimental verification.

Case 4: Similarly, with AVR, it can be seen from Fig. 9 that the LOS issue of Case 3 has been addressed. The VSC can well keep synchronization with the grid during LVRT and the ω_{PLL} rapidly return to the rated value after a fast transient synchronization process.

To further demonstrate the effectiveness of AVR proposed in this letter, a comparative analysis with existing transient stability strategy is performed. The literature [6] proposed an additional damping control method to improve the VSC's transient stability. Fig. 10 shows the control effect comparison between this strategy and AVR.

When the grid voltage drops to 0.05 p.u., I_{df}^{*} and I_{qf}^{*} are set to 0.6 and -0.8 p.u., respectively. According to (1), $T_{\mathrm{v}}^{*}>T_{\mathrm{v}}$, so no equilibrium point exists in the VSC system. As can be seen from Fig. 10, the additional damping control strategy cannot deal with the condition of lacking equilibrium point and the LOS incident for angular frequency rising occurs, while the proposed AVR strategy can help VSC operate stably to a new equilibrium point.

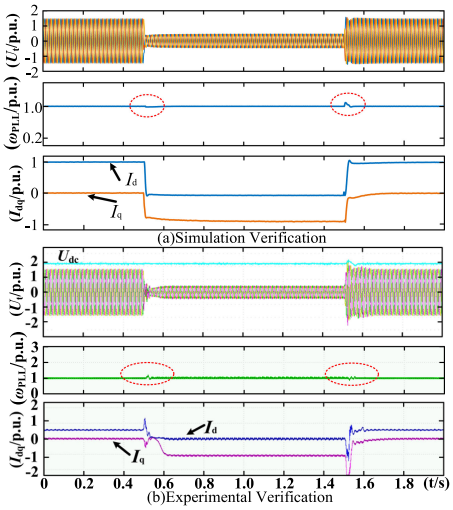

Fig. 9. Simulation and experimental results of Case 4. (a) Simulation verification. (b) Experimental verification.

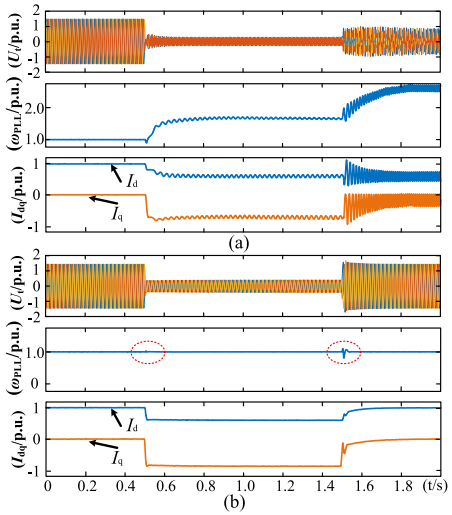

Fig. 10. Control effect comparison. (a) Additional damping control method proposed in [6]. (b) AVR strategy.

Consequently, the simulation and experimental studies nicely demonstrate that the proposed AVR strategy has a significant improvement effect on both the existence of equilibrium points and transient synchronization behaviors of the grid-connected VSC under grid symmetrical fault.

IV. Conclusion

The contribution of this letter is to put forward a transient synchronization stability improvement control strategy based on AVR, which can help the VSC system improve the existence of equilibrium points and transient synchronization behaviors. Both the theoretical analysis and experimental results prove that under the action of AVR strategy, the VSC can avoid transient instability incidents and its LVRT capability can be significantly enhanced under symmetrical grid fault. Finally, considering that the asymmetrical faults are more likely to occur, the control scheme proposed in this letter can also provide a foundation for addressing the VSC's transient synchronization stability issue under asymmetric grid faults.

Appendix

TABLE I
Parameters of the Simulation System

Symbol	Description	Value
P_n	Rate power	2 MW (1 p.u.)
V_n	Rate voltage	690 V (1 p.u.)
V_{dc}	dc-link voltage	1200 V
f_g	Rate frequency	50 Hz
L_f	Grid-side filter inductance	0.25 p.u.
C_f	Filter capacitor	0.15 p.u.
k_p, k_i	PI coefficients of the PLL	1.0, 60
k_{pf}, k_{if}	PI coefficients of the AVR	1.0, 20
SCR	short-circuit ratio	2.2

TABLE II
Parameters of the Experimental VSC System

Symbol	Description	Value
P_n	Rated power	2.0 kW (1 p.u.)
V_n	Rated voltage	220 V (1 p.u.)
f_g	Frequency	50 Hz
L_f	Grid-side filter inductance	5 mH
C_f	Filter capacitor	30 μF
U_{dc}	Reference voltage of DC-link	430V (1 p.u.)
k_p,k_i	PI gains of the PLL	0.8,80
k_{pf}, k_{if}	PI coefficients of the AVR	1.0, 10
SCR	short-circuit ratio	2.2

References

[1] *Technical Rule for Connecting Wind Farm to Power System*, Chinese Standard GB/T 19963-2011, 2011.

[2] Ö. Göksu, R. Teodorescu, C. L. Bak, F. Iov, and P. C. Kjær, "Instability of wind turbine converters during current injection to low voltage grid faults and PLL frequency based stability solution," *IEEE Trans. Power Syst.*, vol. 29, no. 4, pp. 1683–1691, Jul. 2014.

[3] H. Wu and X. Wang, "Design-oriented transient stability analysis of grid-connected converters with power synchronization control," *IEEE Trans. Ind. Electron.*, vol. 66, no. 8, pp. 6473–6482, Aug. 2019.

[4] H. Yuan, H. Xin, L. Huang, Z. Wang, and D. Wu, "Stability analysis and enhancement of type-4 wind turbines connected to very weak grids under severe voltage sags," *IEEE Trans. Energy Convers.*, vol. 34, no. 2, pp. 838–848, Jun. 2019.

[5] X. He, H. Geng, R. Li, and B. C. Pal, "Transient stability analysis and enhancement of renewable energy conversion system during LVRT," *IEEE Trans. Sustain. Energy*, vol. 11, no. 3, pp. 1612–1623, Jul. 2020.

[6] Y. Liu *et al.*, "Transient stability enhancement control strategy based on improved PLL for grid connected VSC during severe grid fault," *IEEE Trans. Energy Convers.*, vol. 36, no. 1, pp. 218–229, Mar. 2021.

[7] J. Pei, J. Yao, Y. Liu, S. Chen, P. Sun, and S. Huang, "Modeling and transient synchronization stability analysis for PLL-based renewable energy generator considering sequential switching schemes," *IEEE Trans. Power Electron.*, vol. 37, no. 2, pp. 2165–2179, Feb. 2022.

[8] S. Ma, H. Geng, L. Liu, G. Yang, and B. C. Pal, "Grid-synchronization stability improvement of large scale wind farm during severe grid fault," *IEEE Trans. Power Syst.*, vol. 33, no. 1, pp. 216–226, Jan. 2018.